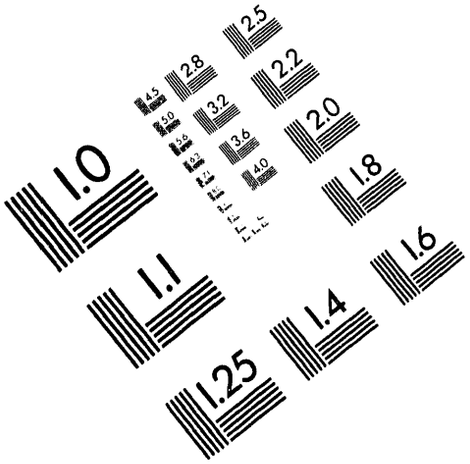

Association for Information and Image Management
1100 Wayne Avenue, Suite 1100
Silver Spring, Maryland 20910
301/587-8202

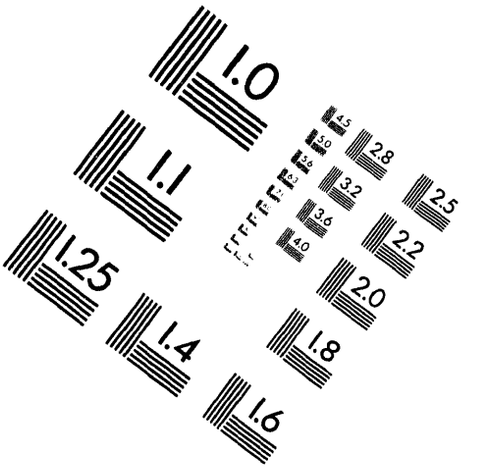

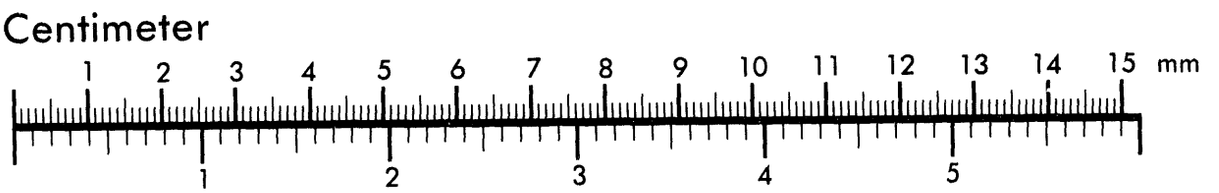

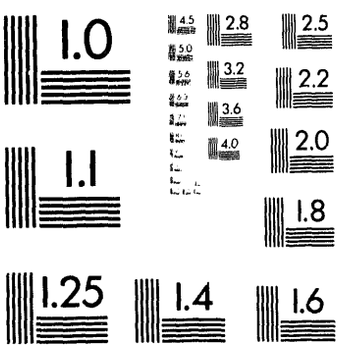

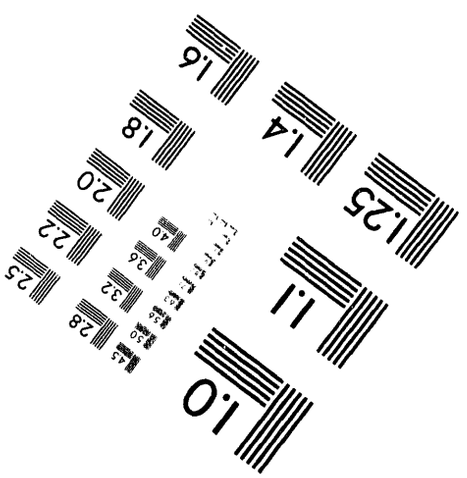

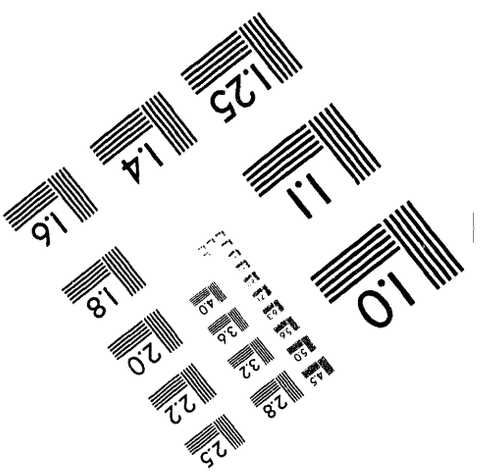

1 of 1

2

Conf-9408123--1

SAND-94-0395C

JANNAF Propulsion Systems Hazards Subcommittee Meeting,
San Diego, California (August 1-5, 1994)

THERMAL, CHEMICAL, AND MECHANICAL COOKOFF MODELING*

M. L. Hobbs, M. R. Baer, and R. J. Gross
Engineering Sciences Center, Sandia National Laboratories†
Albuquerque, New Mexico 87185 USA

ABSTRACT

A Thermally Reactive, Elastic-plastic eXplosive code, TREX, has been developed to analyze coupled thermal, chemical ***and*** mechanical effects associated with cookoff simulation of confined or unconfined energetic materials. Prior modeling has focused on the onset of runaway combustion behavior based only on thermal-chemistry effects with little regard to mechanical behavior such as thermal expansion or internal pressurization of the energetic material. Recent experimental work has suggested that a small degree of decomposition leads to significant pressure buildup.[1] In confined systems, pressure buildup precedes thermal runaway, and unconfined energetic material expands to relieve high stress. This work presents the development of a constitutive material stress-strain model which is incorporated into a fully coupled one-dimensional, thermal-chemical-mechanical computer code (TREX) to simulate cookoff of energetic materials.

A micromechanical constitutive model has been developed based on nucleation, decomposition chemistry, and elastic/plastic mechanical behavior of a material with a distribution of internal defects represented as clusters of spherical inclusions. A local force balance, with mass continuity constraints, forms the basis of the model requiring input of temperature and reacted gas fraction of the energetic material. This constitutive material model has been incorporated into a quasistatic mechanics code, SANTOS,[2] as a material module which predicts stress history associated with a given strain history. The thermal-chemical solver, XCHEM,[3,4] has been coupled to SANTOS[2] to provide temperature and reacted gas fraction. Predicted spatial history variables include temperature, chemical species, solid/gas pressure, solid/gas density, local yield stress, and gas volume fraction.

One-Dimensional Time to eXplosion (ODTX) experiments for TATB and PBX 9404 (HMX and NC) are simulated using global multistep kinetic mechanisms[5] and the reactive elastic-plastic constitutive model.[6] Pressure explosions, rather than thermal runaway, result in modeling slow cookoff experiments of confined conventional energetic materials such as TATB.[7] For PBX 9404, pressure explosions also occur at fast cookoff conditions because of low temperature reactions of nitrocellulose resulting in substantial pressurization. A demonstrative calculation is also presented for reactive heat flow in a hollow, propellant-filled, stainless steel cylinder, representing a rocket motor. This example simulation shows extrusion of the propellent which suggests that the energetic material becomes shock sensitive as a result of slow cookoff.

INTRODUCTION

Determination of decomposition mechanisms and rate laws, thermophysical properties of thermally-damaged materials, constitutive stress-strain laws for degraded materials, and benchmark experiments to assess the time and violence of confined and unconfined cookoff events remain major unsolved problems. Cookoff modeling of confined and unconfined energetic materials requires fully coupled modeling of thermal, chemical and mechanical effects. In the past, modeling has focused on the prediction of thermal runaway with little regard to mechanical effects such as thermal expansion or pressurization. An overview of thermal initiation of explosives is given by Frank-Kamenetskii[8] and Zinn and Mader.[9] Zinn and Rogers[10] discuss a simplified pressurization model based on a gaseous equation of state (EOS). Zinn and Rogers[10] assumed no strain of the energetic material. This assumption only considers leading order effects for fast cookoff and is incorrect for slow cookoff. Such analyses are strictly limited to thermal runaway and do not correctly address the complex issues related to material mechanical response.

The present work enhances our capabilities to understand the coupling between thermochemistry and mechanics by describing a, stress-strain constitutive law for a Reactive Elastic-Plastic (REP) material. This algebraic

---

* Approved for public release; distribution is unlimited.

† This work performed at Sandia National Laboratories supported by the U.S. Department of Energy under contract DE-AC04-94AL85000

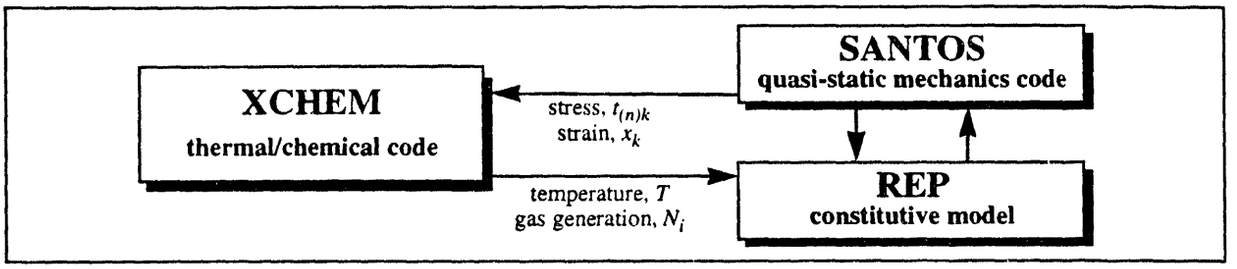

Figure 1. Schematic of TREX showing coupling between XCHEM and SANTOS.

constitutive law is used as a material module in a quasistatic mechanics code, SANTOS,[2] coupled to a thermal chemistry code, XCHEM.[3,4] This one-dimensional thermal, chemical, and mechanical code is called TREX (Thermally Reactive, Elastic-plastic eXplosive code). Although energetic materials are often contained in complex systems with 3-D multimaterial geometries, risk assessment analysis are often based on simplified modeling. Furthermore, insight regarding the incorporation of mechanics into multidimensional finite element analyses, being developed at Sandia National Laboratories, can be gained from studies in one-dimension.

ONE-DIMENSIONAL THERMAL, CHEMISTRY, AND MECHANICS MODEL

TREX is a one-dimensional code composed of three modules. These modules consist of a thermal/chemistry solver, XCHEM,[3,4] a static mechanics code, SANTOS,[2] and the constitutive material model, REP, as shown in Figure 1. TREX uses an operator splitting technique in which the thermal/chemical fields are advanced using a fixed mechanics field; the mechanics are then advanced over the same time interval using the updated thermal/chemical fields. This technique provides for a rapid solution since the mechanical solver is inactive during the small time steps required by the thermal/chemistry solver. The thermal chemistry solver is an adaptive gridding method-of-lines code and the mechanics solver is a finite element code with a fixed number of elements. Mesh interpolation is required to communicate the temperature and reacted fraction from the thermal chemistry code to the quasi-static mechanics code. The REP constitutive model is incorporated as a material module for SANTOS to determine stress history associated with a given strain history. Strain is passed back to XCHEM in the form of an expanded or contracted grid. Gaps may form between layers of materials which are used to determine thermal contact resistance between layers. Stress is communicated from SANTOS to XCHEM as mixture pressure which may ultimately couple to pressure dependent combustion mechanisms. Predicted spatial history variables include temperature, chemical species, principle stress, engineering strain, solid/gas pressure, solid/gas density, local yield stress, and gas volume fraction. The gas volume fraction can be used to calculate the specific surface area if the initial nucleation density and physical sizes of defects of the energetic material are known or can be estimated.

THERMAL/CHEMISTRY SOLVER - XCHEM

General description - The eXplosive CHEMical kinetics code, XCHEM,[3,4] has been developed to solve the reactive diffusion equations associated with thermal ignition of energetic materials. This method-of-lines code uses a stiff numerical method and adaptive meshing to resolve relevant combustion physics. Solution accuracy is maintained between multilayered materials consisting of blends of reactive components and/or inert materials. Phase change and variable properties are included in multi-layer one-dimensional slab, cylindrical, and spherical geometries. Temperature-dependent thermal properties have been incorporated and the modification of thermal conductivities to include decomposition effects are estimated using solid/gas volume fractions determined by species fractions. Gas transport properties, including high-pressure corrections, have also been included. Time-varying temperature, heat flux, convective and thermal radiation boundary conditions, and layer-to-layer contact resistances have also been implemented.

Conservation equations - The conservation equations for energy and species form the foundation of the thermal-chemistry solver as shown in Table 1. The source term in the energy equation (Table 1, Eq. 1) is described by global or elementary reaction mechanisms as given by Eq. (2)-(6) in Table 1. Input parameters include geometry, physical dimensions of layers, initial temperature of layers, start and finish times, gap distances between layers, gray body emissivities of gap surfaces, thermal conductivity of the gases in the gap, percentage of unclosed gap surface area, temperature dependent thermal conductivity, temperature dependent specific heat, phase change temperature,

latent enthalpy, density, volume fraction of reactive or nonreactive materials in each layer, time dependent boundary temperature or flux, steric factors, pre-exponential factors, activation energies, endothermic and/or exothermic reaction enthalpies, concentration exponents, and stoichiometric coefficients. Calculated quantities include spatial histories of temperature and gas species or reacted gas fraction. Details on the energy equation, chemical species rate equations; example chemical decomposition mechanisms (including physical properties) for HMX, NC, RDX, TATB, and TNT; effective capacitance method for phase change; mixture rules for thermal conductivity and heat capacity, contact resistance formulation, and numerical solution technique can be found in Reference 4. Gap formation and closure is not calculated directly in XCHEM. Rather, the quasi-static mechanics code discussed in the following section is used to determine transient gap distances.

Table 1 Equation set for thermal-chemistry solver, XCHEM[3,4]

Energy equation (thermal/chemical operator)	$\rho C_p \frac{\partial T}{\partial t} = \lambda \nabla^2 T + S_T$	(1)
Reaction source	$S_T = \sum_{i=1}^{I} \sum_{j=1}^{J} \mathcal{H}_{ij} \rho_i r_{ij}$	(2)
General reaction scheme	$\sum_{i=1}^{I} \nu'_{ij} \mathcal{M}_i \rightarrow \sum_{i=1}^{I} \nu''_{ij} \mathcal{M}_i \quad , \quad j = 1, \ldots J$	(3)
Reaction rate	$r_j = k_j(T) \prod_{i=1}^{I} N_i^{\mu_{ij}} \quad , \quad j = 1, \ldots J$	(4)
Arrhenius kinetic coefficients	$k_j(T) = T^{\beta_j} A_j \exp(-E_j/RT)$	(5)
Conservation of species	$dN_i/dt = \sum_{j=1}^{J} \nu_{ij} r_j \quad , \quad i = 1, \ldots I$	(6)

Nomenclature

A	pre-exponential factor (1/s)	λ	heat conductivity (cal/cm-s-K)	R	Gas constant, (cal/mol-K)
β	steric coefficient	$\mathcal{M}$	chemical symbol for i^{th} species	ρ	density, (g/cm^3)
Cp	heat capacity (cal/g-K)	μ	concentration exponent	S_T	Reaction source term, (cal/cm^3-s)
E	activation energy (cal/mol)	N	species progress variable		
$\mathcal{H}$	energy release (cal/g)	ν'	reactant stoichiometric coefficient	t	time, (s)
I	number of species	ν''	product stoichiometric coefficient	T	temperature, (K)
J	number of reactions	ν	reaction rate coefficient		
k	kinetic coefficient (1/s)	r	reaction rate, (1/s)		

QUASI-STATIC MECHANICS SOLVER - SANTOS

General description - The finite element code, SANTOS,[2] is used to determine quasistatic, large deformation, nonlinear response of planar or axisymmetric solids. Elastic-plastic and creep behavior are included as finite strain constitutive material models. Thermal expansion can be simulated for reactive materials. Quasi-steady solution of the mechanics is obtained using a self-adaptive dynamic relaxation scheme based on explicit central difference pseudo-time integration and artificial damping. Gap formation is implemented in the finite element solution by using a master-slave algorithm for sliding interfaces.

Conservation equations - The conservation equations for energy and mass form the foundation of the quasi-static mechanics solver as given in Table 2.[11,12] The energy equation given in Table 2 states that the variation of total

internal energy is equal to the sum of the surface work and work by body forces. (Total energy conservation over a time interval is enforced with the sequential solution of the equations given in Tables 1 and 2. The thermal/chemical energy equation is first resolved assuming the mechanics field is unchanged, then the mechanical energy equation is solved assuming frozen thermal/chemical fields. Thus, on a time step by time step basis, all thermal, chemical and mechanical effects are included as a fully coupled model.)

All variations are subject to conservation of mass. Common stress strain relationships such as elastic-plastic, viscoelastic, and elastic-plastic power law hardening materials are described in Reference 13. In the present work, the elastic-plastic constitutive model is used for inert structural materials. This model uses standard von Mises yield with kinematic and isotropic hardening. The derivation of the elastic-plastic constitutive model is scattered throughout the literature; and, the underlying assumptions and numerical approximations can be found in Reference 13. A new algebraic stress-strain constitutive law for a reactive, elastic-plastic material is discussed in the following section.

Table 2 Equation set for quasi-static mechanics solver, SANTOS[2]

Energy equation (mechanics operator)	$\delta\int_{\mathcal{V}}\rho e\,dv = \oint_{S} t_{(n)k}\delta x_k\,da + \int_{\mathcal{V}}\rho f_k\delta x_k\,dv$ Variation in internal energy = surface work + work by body force	(1)
Conservation of mass	$\delta\int_{\mathcal{V}}\rho\,dv = 0$	(2)
Constitutive stress-strain law	See Table 3 for reactive materials and Ref. 13 for structural materials	(3)

Nomenclature

a	area (cm^2)	f_k	acceleration (cm/s^2)	$t_{(n)k}$	surface traction ($dynes/cm^2$)
δ	variation symbol (e.g. $\delta x = \partial x/\partial x_k$)	k	direction index	v	volume (cm^3)
		ρ	density (g/cm^3)	$\mathcal{V}$	integration volume
e	specific energy (cal/g)	S	integration surface	x_k	deformation (cm)

REACTIVE, ELASTIC-PLASTIC CONSTITUTIVE MODEL - REP

Physical Observation - Figure 2 shows a 50X magnification of thermally degraded TATB (2,4,6-trinitro-1,3,5-benzenetriamine) showing evidence of macroscale pore formation.[1] The fully-pressed sample was confined with O-rings, heated 5 K/minute to 523 K, and held at 523 K for 1 hour before loss of confinement at ~100 atm. The total mass loss was estimated to be ~5%. Thermal decomposition of energetic materials produced gaseous products which accumulate in defects or nucleation sites and contribute to local pressurization. This physical observation motivates the development of a constitutive model based on bubble nucleation theory.

Conceptual Model - A region of space or element filled with a collection of nucleation sites taken to be spherical inclusions is depicted in Figure 2. The unit cell in this element is used to model micromechanical bubble evolution in a porous reactive material. The time varying internal and external radius of the sphere are designated as a and b, respectively. In this simplified model, a represents a statistically averaged bubble defect size and b is related to the average distance between defects. The inner sphere contains gas at the initial density, ρ_g^o, which becomes supplemented by combustion gases that mechanically load the skeletal condensed-phase mass of the outer shell at an unstressed density of ρ_c^o. The initial inner, a_o, and outer, b_o, sphere radius can be determined from the initial gas volume fraction, ϕ_o, and the nucleation site density, N_o. An estimate of the initial porosity of the reactive material, ϕ_o, is required for the algebraic stress-strain relationship. The specific surface area of the thermally damaged reactive material can be determined from a and b.

Model Equations and Assumptions - The micromechanical model is given by the six algebraic equations shown in Table 3. These equations describe 1) the conservation of gas mass, 2) the conservation of total mass, 3) the gas-phase equation of state (EOS), 4) the condensed-phase EOS, 5) the force balance between gas pressure, solid

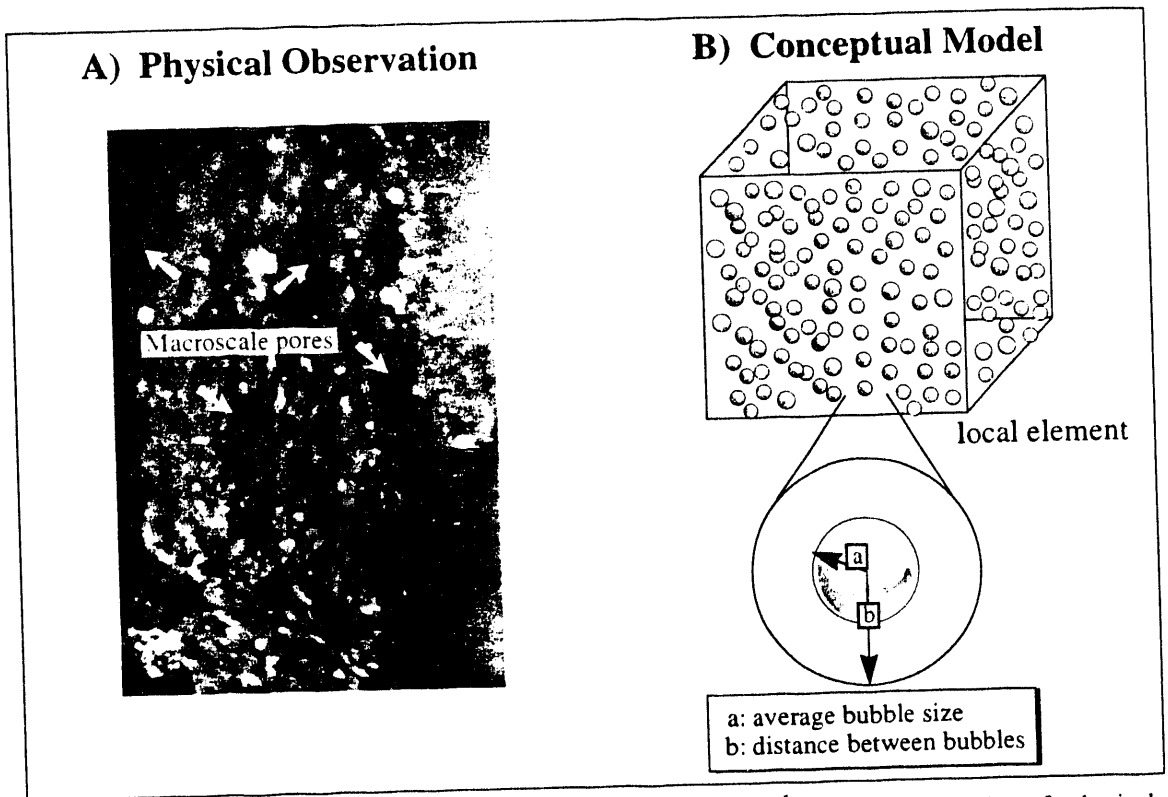

Figure 2. A) Magnification of degraded TATB from Renlund[1] and B) cross-section of spherical shell used to model micromechanical bubble evolution in a porous reactive material.

Table 3. Algebraic equation set for a reactive elastic-plastic constitutive model

Gas mass continuity	$\rho_g = \rho_g^o \phi_o [1 + F(\lambda - 1) + \psi(1/\phi - 1)] / (1 + \varepsilon)$	(1)
Reacted gas fraction	F = (mass of gas prod.)/(initial cond. mass)	(1a)
Material parameter	$\lambda = \left(\rho_c^o / \rho_g^o\right)(1/\phi_o - 1) + 1$	(1b)
Normalized gas mass	$\psi = \rho_g a^3 / \rho_g^o a_o^3 = \lambda - (\lambda - 1)(1 - F)$	(1c)
Gas volume fraction	$\phi = a^3 / b^3$	(1d)
Total mass continuity	$\rho_c = \rho_g (\lambda/\psi - 1) / (1/\phi - 1)$	(2)
Gas-EOS	$P_g = z \rho_g RT / M_w$	(3)
BKW compressibility	$z = 1 + xe^{\beta x}$	(3a)
BKW parameter	$x = \rho_g \kappa \sum y_i k_i / M_w (T + \theta)^{\alpha}$	(3b)
Cond.-EOS (Mie-Grüneisen)	$P_c = \rho_c \Gamma_c C_v \xi (T - T_o) + K_T \left[(\rho_c / \rho^o{}_c)^N - 1 \right] / N$	(4)
Force balance	$\sum \text{forces} = 0 = -P_g + P_g^o + P_c - 2/3 \cdot Y \ln(1/\phi)$	(5)
Mixture pressure definition	$-\sigma = \{\phi P_g + (1 - \phi) P_c\} i$	(6)

pressure, and yield stress of the skeleton solid, and 6) the mixture pressure. The conservation equations for energy and species are not part of the micromechanics model since temperature (T) and the reacted gas fraction (F) are provided by the thermal/chemical solver (XCHEM). Assuming T and F are known, the six equations have seven unknowns, producing a stress-strain relationship. The seven unknown parameters in the equation set in Table 3 are 1) principle stress, σ, 2) engineering strain, ε, 3) gas density, ρ_g, 4) condensed-phase density, ρ_c, 5) gas pressure, P_g, 6) condensed-phase pressure, P_c, and 7) gas void fraction, ϕ. Closure of the model is obtained by the determination of a stress field consistent with material strain as resolved by the finite element solver SANTOS.

The micromechanical model assumes that 1) defects are spherical, 2) gas- and condensed-phase temperatures are equal within elements, 3) gas- and condensed-phase densities are uniform within elements, 4) the material responds instantaneously to applied forces (i.e., viscous effects are negligible), 5) bubble inertial effects are negligible, 6) momentum exchange due to reaction is small, and 7) the reactive material is isotropic. The model is general such that any appropriate EOS can be chosen for the gas- and condensed-phases. Herein, the BKW-EOS and Mie-Grüneisen EOS are chosen for the gaseous EOS and condensed EOS, respectively. The BKW-EOS performs well at high gas pressures and is well-behaved at high gas densities. The Mie-Grüneisen EOS accounts for thermal expansion and compressibility of the skeleton solid. A factor, ξ, modifies thermal expansion material properties for thermally degraded material.

The stress-strain relationship given in Table 3 is implicit in porosity, ϕ. For a given ε, F, ρ_g^o, ρ_c^o, ϕ_o, and yield, Y; ϕ, and consequently $-\sigma$, can be determined iteratively, or with a general root finding algorithm. The yield stress, $G(\phi, Y)$, given by Carroll and Holt,[14] was modified to account for elasticity as follows:

$$G(\phi, Y) = \min[2/3 \cdot Y \ln(1/\phi), E(\phi_{crit} - \phi)] \tag{1}$$

$$E = 3K_T(1 - 2\nu) \tag{2}$$

where Y, E, K_T, and ν represent yield strength, Young's modulus, bulk modulus, and Poisson's ratio, respectively. Yield functions are usually written in the form $\psi = \sigma - G$ where $\psi = 0$ defines a yield surface in stress space. Plastic deformation is included as a micromechanical deviatoric stress. At the macroscale, only principle stresses are considered, *i.e.* $\sigma = \frac{1}{3}\sigma : i$. In the present work, Poisson's ratio is assumed to be equal to one third (1/3) since Poisson's ratio for most energetic materials ranges between 0.2 and 0.4. The yield stress is set to zero when the gas volume fraction is greater than a critical gas volume fraction, ϕ_{crit}. The critical gas volume fraction, ϕ_{crit}, is a history variable which accounts for hysteresis effects (loading vs unloading) by keeping track of the minimum value of the gas volume fraction, ϕ. The critical gas volume fraction is always less than or equal to the gas volume fraction which no longer supports plastic deformation, ϕ_{yield}^{max}. The yield stress, Y, is assumed to be linearly dependent on temperature below the melting point, and zero above the melting point.

MODEL APPLICATIONS

As sample TREX calculations, two types of problems were chosen: 1) confined ODTX cookoff[5] of TATB and PBX 9404 and 2) an unconfined rocket motor exposed to a fire. All thermal/chemical parameters for TATB and PBX 9404 (94/3/3 weight percent HMX/NC/inert) were taken unchanged from References 3-5 with the exception of the reaction enthalpy for the NC mechanism. The reaction enthalpy for the NC mechanism in References 3-5 was set to one-half the overall heat of reaction of nitrocellulose to mimic the inert binder in PBX 9404. Rather than partition reaction enthalpy to the binder in this manner, we chose to treat the binder as nonreacting. The polymer binder in PBX 9404 (3% by weight) is modeled assuming the same thermal and mechanical properties as nonrigid polyvinyl chloride. Well-known thermal and mechanical properties are used for aluminum and stainless steel. The mechanical parameters used in the REP model for the reactive materials can be found in Reference 6 and 7. The initial gas volume fraction was assumed to be 0.05 for all cases. The factor, ξ, was set to 0.7 for the confined explosives to obtain optimal agreement between ODTX data and TREX predictions. This factor was set to 1.0 for the unconfined rocket motor.

CONFINED EXPLOSIVES

In the spherical ODTX experiments, McGuire and Tarver[5] modeled preheated aluminum anvils confining 1.27 cm diameter spherical samples of explosive. Heaters controlled the temperature of the anvils to ±0.2 K, and the

primary measurement was the time to "explosion" which represented confinement failure. The anvil confinement hydraulically sealed to 1500 atm.

The spherical ODTX experimental data and TREX calculated results are shown in Figure 3 for TATB and PBX 9404. Typically, the logarithm of time to confinement failure versus the reciprocal of the surface temperature T_f, is linear over a large region, but sharply bends upward near the critical temperature, T_c, as shown in Figure 3.A for TATB. The dashed line represents calculated thermal runaway, the solid line represents the time when pressure venting is assumed to occur, and the symbols correspond to experimental data. For conditions of fast heating, thermal runaway and mechanical failure coincide. However, for slow cookoff, failure of confinement is largely due to thermal-mechanical response of the energetic material.

For PBX 9404, a plateau at fast cookoff conditions is apparent in Figure 3.B. This plateau results from low temperature reactions of nitrocellulose resulting in substantial pressurization. To our knowledge, the features in Figure 3 have never before been calculated with a true estimate of confinement rupture. Tarver[15] assumed a heat release for NC that was twice as large as calorically possible (excluding any cross-catalytic chemistry effects) and suggested that the plateau was entirely a thermal response. The two-step kinetic mechanism used for the TREX calculations may be inadequate to capture the abrupt change in failure times shown for both the aged and new PBX 9404 data shown in Figure 3.B. The experimental data of Chen and Brill[18] suggest that the kinetics for fast heating rates are different from those measured at slow heating rates. Although a change in mechanism with temperature may explain the abrupt change in failure times, small amounts of additives may also effect results. For example, the stabilizer used in PBX 9404, 0.1% diphenylamine, has a noticeable effect on the ODTX results as shown in Figure 3.B; the aged PBX 9404 reacts sooner than the new PBX 9404. The kinetic rate mechanisms used in TREX were obtained from the original fits to the ODTX data which did not filter out mechanical behavior or pressure effects in the chemical rates. Clearly much improved kinetic rates are warranted to explain the time to failure observed for PBX9404. However, these calculations demonstrate the importance of including mechanical effects during slow cookoff of confined explosives, especially in benchmark experiments used to assess chemical kinetics.

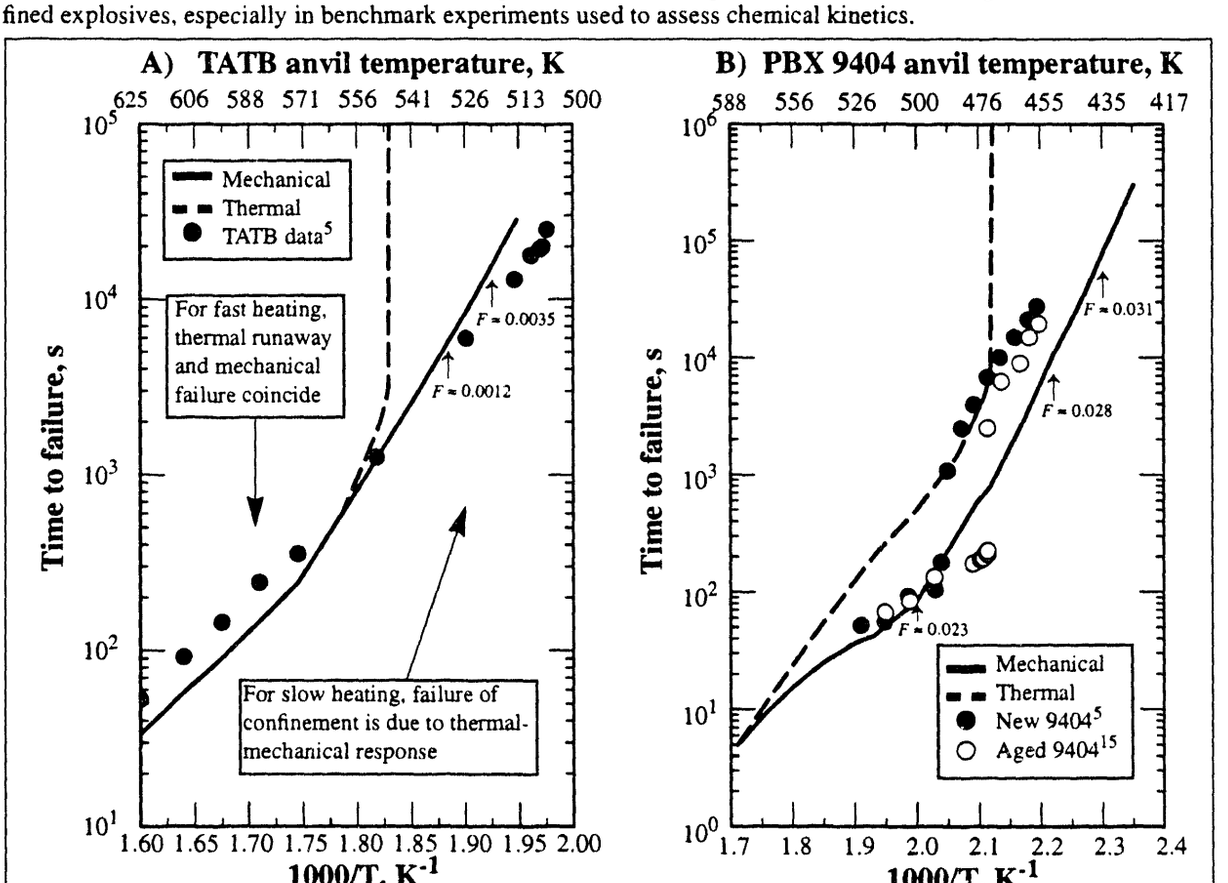

Figure 3 Calculated and experimental time to failure for 1.27 cm diameter spheres of **A**) TATB and **B**) PBX 9404

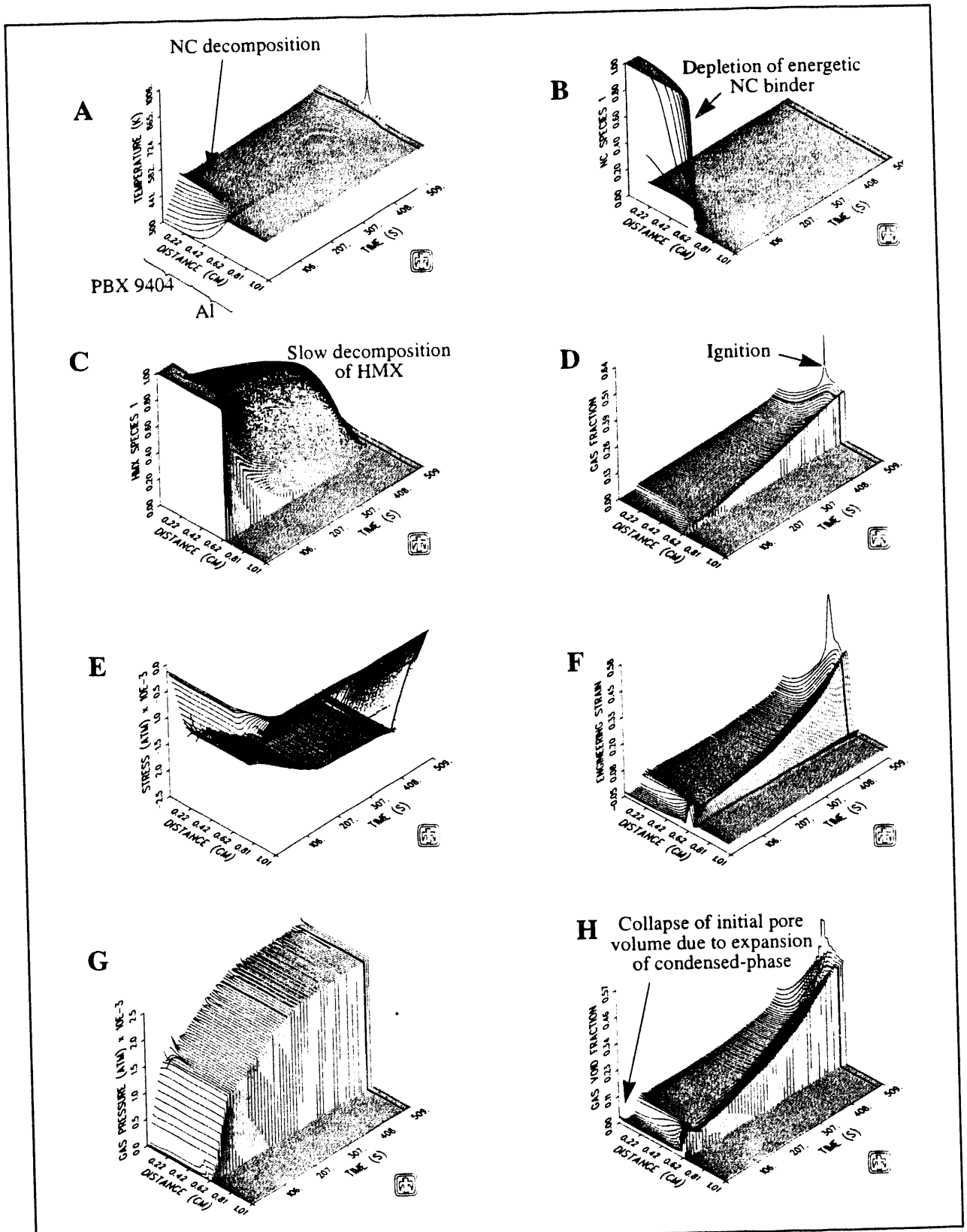

Figure 4 Spatial histories of A) temperature, B) nitrocellulose, C) HMX, D) reacted gas fraction, E) principle stress, F) engineering strain, G) gas pressure, and H) gas volume for a 1.27 cm diameter spherical ODTX simulation with a 500 K boundary temperature, respectively.

Figures 4 displays the spatial temperature, gas fraction, principle stress, and engineering strain history for the PBX 9404 ODTX simulation with a 500 K boundary temperature. Significant nitrocellulose decomposition is shown at early times resulting in plastic deformation of the energetic material. As the energetic material reacts, pressure caused by increasing temperature (material thermal expansion) and gas production causes the material to densify. The compressed material causes collapse of the inclusions resulting in a decreased gas-phase volume fraction until gas generation is sufficient to cause the defects to grow in extent.

UNCONFINED ROCKET MOTOR

As an additional calculation, reactive heat flow with mechanics is considered in a hollow stainless steel cylinder filled with a propellant composed of 45/50/5 weight percent Al/HMX/NC. The aluminum in the propellent is treated as nonreactive and acts as a heat sink and material stiffener. The physical configuration with the imposed internal/external transient ambient temperature is given in Figure 5. The external and internal convective coefficients are 0.001 and 0.0005 cal/cm^2-s-K, respectively. The kinetic and thermal properties, reaction mechanisms, and mechanical properties for the reactive materials are taken from References 3-7 respectively. Typical thermal and mechanical properties are used for aluminum and stainless steel.

Figure 5.C shows gap formation and gap closure due to transient heating of the stainless steel shell and subsequent expansion of the propellant. Gaps between layers inhibit heat transfer. For example, the onset of NC decomposition, apparent in Figure 6, occurs approximately 100 s earlier when gap formation is not considered.

As shown in Figures 6 and 7, the propellent foams and extrudes a distance of 5 cm to fill the bore. These results are consistent with large scale cookoff experiments in which foaming propellent was observed to extrude out of a rocket nozzle prior to ignition.[16] In these experiments, an internal video revealed an RDX-based propellent which nearly doubled in volume during a slow cookoff test. Approximately 1/3 to 1/2 of the propellant mass extruded out of the nozzle. As the propellent was extruding out the nozzle, intermittent bursts of gas were released

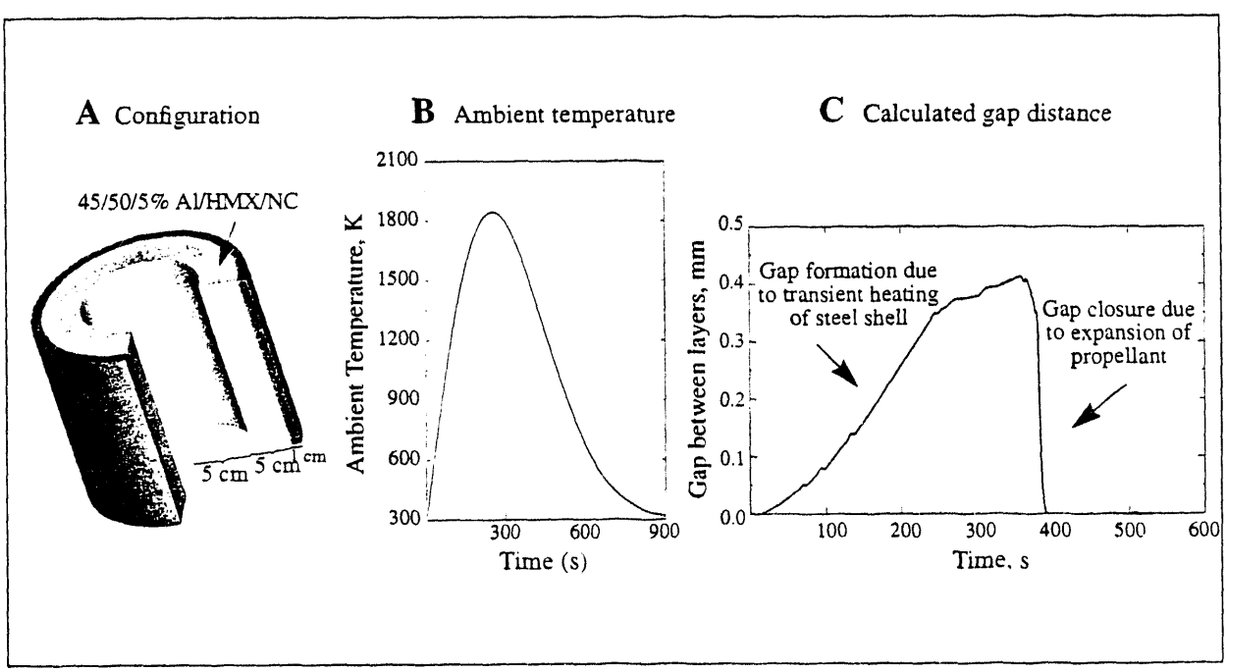

Figure 5 A) Physical configuration, B) internal/external transient ambient temperature for demonstrative thermal, chemical and mechanical calculation, and C) calculated gap distance between propellant and stainless steel case.

through the motor nozzle, indicating that large pockets of gas were generated within the propellent. The extruded propellant was ignited by the oven heating elements, burned unconfined for 16 seconds before reaching the confined rocket motor. The motor then exploded, and was thought to have partially detonated. The increased gas volume fraction leads to the production of voids which act as a potential site for "hot-spots" which enhance the shock sensitivity of the propellant.[17]

During the heating cycle, significant geometrical changes occur which alter heat flow paths. Geometric modification of the system include the formation of gaps and the expansion of material. For example, Figure 6 displays the spatial histories of temperature, parent species nitrocellulose, parent species HMX, and reacted gas fraction for the rocket motor. As pressure increases due to gas formation at the edges of the energetic material, the propellent expands to relieve this stress. Figure 7 displays spatial histories of principle stress, engineering strain, gas pressure, and gas volume fraction. Once the bore is filled with propellent, the problem becomes multidimensional. Hence, this calculation was not taken to the thermal ignition point.

In Figure 7.A, considerable stress rise in the stainless steel case occurs between 500 s and 560 s. These unphysical stresses are due to the high residual numerical error in the quasistatic mechanics calculation. This high residual error is caused by difficulties in numerical convergence near slidelines. Solution fields near slidelines are not continuous and are notoriously difficult to resolve.[2] Most of this error is located in the stainless steel case. The stress field in the energetic material is due entirely to thermal expansion and pressure due to gas generation. Figure 7.A and 7.C show a uniform stress field until a significant amount of gas is produced. The gas pressure required to overcome the propellent inertia is approximately 35 atm. The stress at the interface between the propellant and the bore is essentially zero.

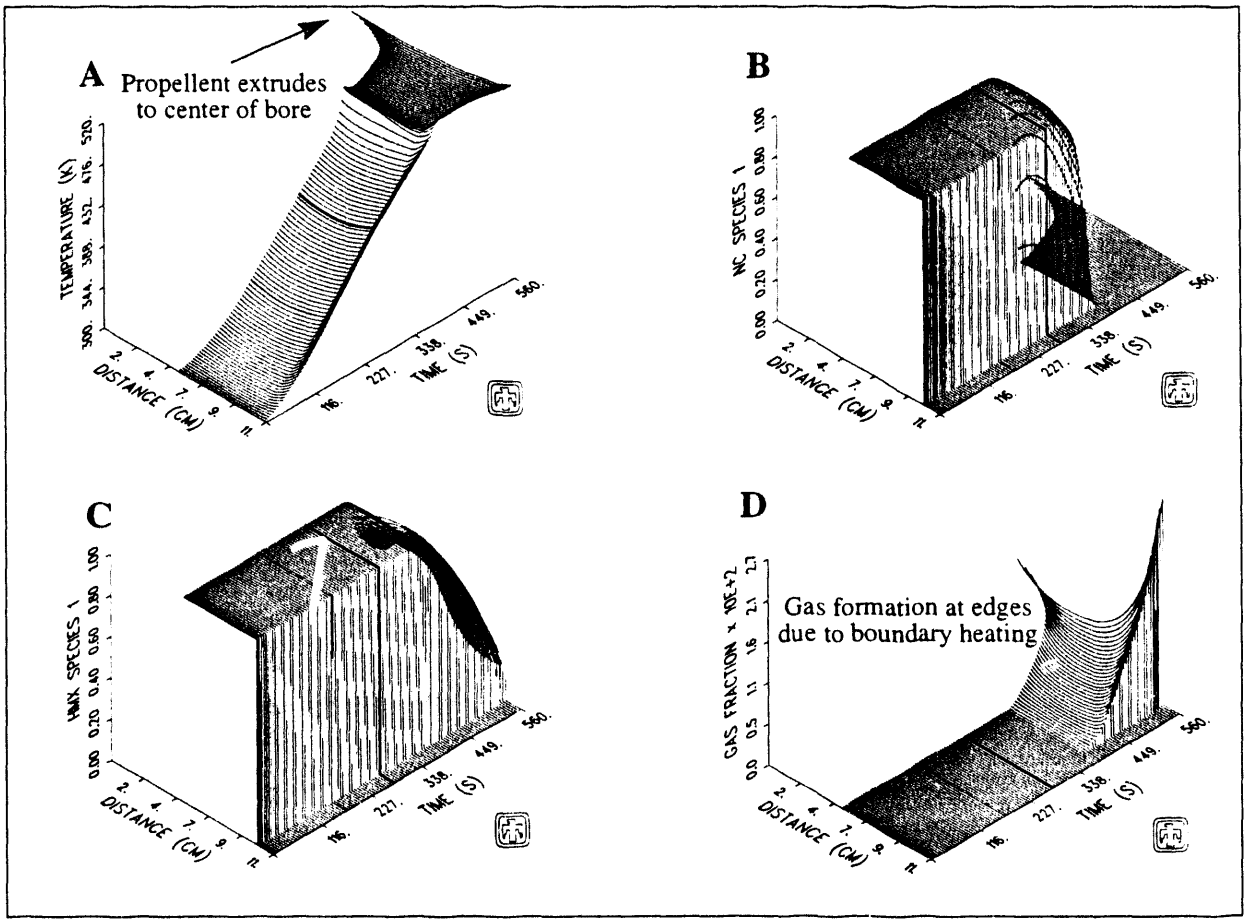

Figure 6 Spatial histories of A) temperature, B) nitrocellulose, C) HMX, and D) reacted gas fraction for the rocket configuration shown in Figure 5.A.

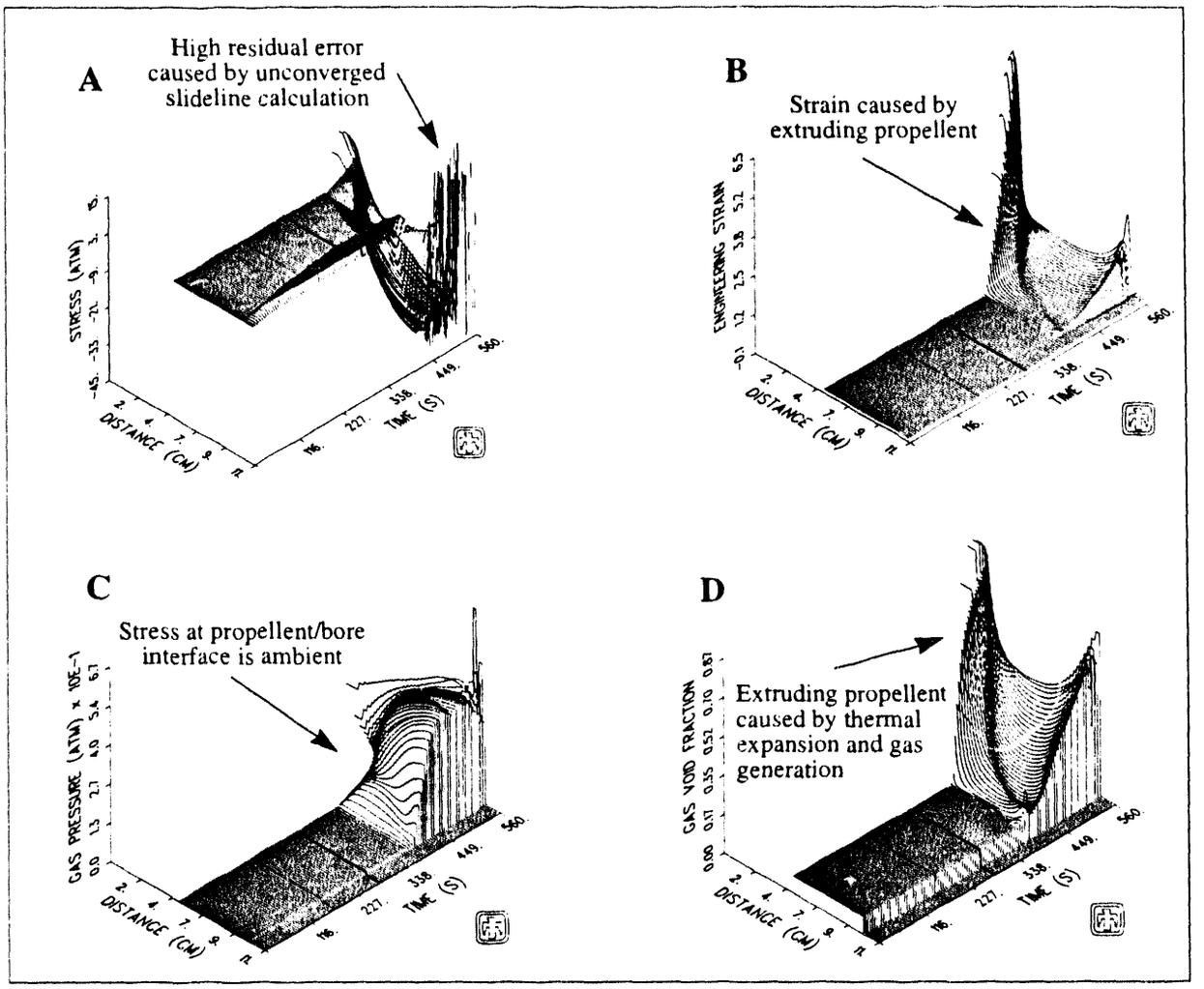

Figure 7 Spatial histories of A) principle stress, B) engineering strain, C) gas pressure, and D) gas volume fraction for the rocket configuration shown in Figure 5.

Figures 5-7 illustrate the complex interaction between heat transfer, chemistry, and mechanics. The engineering strain and gas volume fraction spatial history plots shown in Figures 7.B and 7.D are similar. As the propellent is heated on the inner and outer boundaries, gas is generated which increases the gas volume fraction. The material expands to relieve thermal stress causing the gas volume fraction to increase.

SUMMARY AND CONCLUSIONS

This paper summarizes development of a fully coupled thermal, chemical, and mechanical cookoff code called TREX and gives example calculations involving energetic material in both confined and unconfined geometries. A small degree of decomposition has a profound influence on pressure buildup and/or material expansion.

Confined ODTX experiments were simulated as pressure failure at 1500 atm. The spherically confined ODTX simulations compared favorably to experimental data. Slow cookoff is dominated by significant pressure buildup. Even in fast cookoff simulations, small amounts of decomposition products resulted in large pressures. *Mechanics must be considered in cookoff analysis.*

The unconfined system considered reactive heat flow in a hollow steel cylinder representing a rocket motor filled with a propellant composed of Al, HMX, and NC. Transient internal and external radiative/convective boundary conditions represented 5 minutes of exposure to a fire environment followed by cooling. The propellent increased in volume and extruded to the center of the bore. The increase in propellent volume is attributed to gas generation

causing stress which is subsequently relieved by propellent strain. Unlike the confined system which showed significant pressure build-up before ignition, the unconfined motor showed significant extrusion of the propellent, demonstrating that TREX can model large deformation problems. Large deformation has been observed in cookoff testing whereby the propellent was seen to extrude out of the rocket nozzle.[16]

TREX was developed as a one-dimensional analysis tool with the goal of understanding the coupling between thermal-chemical and mechanics codes, and to assess the REP model. The model can be applied to more complex and computationally demanding multidimensional analysis for simplified studies. The methodology in coupling thermal-chemistry with mechanics in one-dimension with the constitutive material model, REP, will apply directly to multi-dimensional finite analysis codes currently in development at Sandia National Laboratories.

REFERENCES

1. Renlund, A. M., personal communication, Sandia National Laboratories, Albuquerque, New Mexico (1994).
2. Stone, C. M., "SANTOS - A Two-Dimensional Finite Element Program for the Quasistatic, Large Deformation, Inelastic Response of Solids," SAND90-0543, Sandia National Laboratories, Albuquerque, New Mexico, unpublished personal communication (1994), for more information see Stone, C. M., Krieg, R. D., and Beisinger, Z. E., "SANCHO A Finite Element Computer Program for the Quasistatic, Large Deformation, Inelastic Response of Two-Dimensional Solids," SAND84-2618, UC-32 (1984).
3. Hobbs, M. L., Baer, M. R., and Gross, R. J., "Modeling Ignition Chemistry," *JANNAF Systems Hazards Meeting*, Fort Lewis, Washington (May 10-14, 1993).
4. Gross, R. J., Baer, M. R., and Hobbs, M. L., "XCHEM-1D, A Heat Transfer/Chemical Kinetics Computer Program for Multilayered Reactive Materials," SAND93-1603, Sandia National Laboratories, Albuquerque, NM (November 1993).
5. McGuire, R. R. and Tarver, C. M., "Chemical Decomposition Models for the Thermal Explosion of Confined HMX, TATB, RDX, and TNT Explosives," *Seventh Symposium (International) on Detonation*, NSWC MP 82-334, 56 (1981).
6. Hobbs, M. L., Baer, M. R., and Gross, R. J., "A Constitutive Mechanical Model for Energetic Materials" *Twentieth International Pyrotechnics Seminar*, Colorado Springs, Colorado, IIT Research Institute, Chicago, Illinois (1994).
7. Gross, R. H., Baer, M. R., and Hobbs, M. L., "Mechanical Effects in Cookoff Modeling," *Twentieth International Pyrotechnics Seminar*, Colorado Springs, Colorado, IIT Research Institute, Chicago, Illinois (1994).
8. Frank-Kamenetskii, D. A., *Diffusion and Heat Exchange in Reaction Kinetics*, Academy of Sciences of the USSR, 1st ed. (1945), *Nauka*, Moscow, 2nd ed. (1967), Princeton University Press, Princeton New Jersey, Translation (1955).
9. Zinn, J. and Mader, C. L., "Thermal Initiation of Explosives," *J. of Applied Physics*, **31** (2), 323 (1960).
10. Zinn, J. and Rogers, R. N., "Thermal Initiation of Explosives," *J. Phys. Chem.*, **66**, 2646 (1962)
11. Truesdell, C. and Toupin, R., "The Classical Field Theories," in *Encyclopedia of Physics*, Vol. **III/1**, Edited by Flügge, S., Springer-Verlag, Berlin, Germany, 596 (1960).
12. Eringen, A. C., *Mechanics of Continua*, second edition, Robert E. Krieger Publishing Company, Malabar, Florida, 142 (1980).
13. Taylor, L. M. and Flanagan, D. P., "PRONTO 3D A Three-Dimensional Transient Solid Dynamics Program," SAND87-1912, UC-32, Sandia National Laboratories, Albuquerque, New Mexico (1992).
14. Carroll, M. M. and Holt, A. C., "Static and Dynamic Pore-Collapse Relations for Ductile Porous Materials," *J. Appl. Phys.*, **43** (4), 1626 (1972).
15. Tarver, C. M., personal communication, Lawrence Livermore National Laboratory, California (1993).
16. Diede, A., Appendix D, "Nonconventional Cookoff Testing of Rocket Motors," 19D, in *Initial Development and Evaluation of a Retrofittable Multi-Hazard Mitigation System for Rocket Motors*, NWC TP 6849, Naval Weapons Center, China Lake, California (1990).
17. Kang, J., Butler, P. B., Baer, M. R., "A Thermomechanical Analysis of Hot Spot Formation in Condensed-Phase, Energetic Materials," *Combustion and Flame*, **89**, 117 (1992).
18. Chen, J. K., and Brill, R. B., "Thermal Decomposition of Energetic Materials 50. Kinetics and Mechanism of Nitrate Ester Polymers at High Heating Rates by SMATCH/FTIR Spectroscopy," *Comb. Flame*, **85**,479 (1991).

DATE
FILMED
9/28/94

END